Received: 8 June 2023 | Revised: 4 July 2023 | Accepted: 5 July 2023

DOI: 10.1002/ntls.20230015

RESEARCH ARTICLE

Natural Sciences

Foray into the topology of poly-bi-[8]-annulenylene

Varadharajan Muruganandam[1,2] | **Manas Sajjan**[2,3] | **Sabre Kais**[1,2,3]

[1]Department of Physics, Purdue University, West Lafayette, Indiana, USA

[2]Purdue Quantum Science and Engineering Institute, Purdue University, West Lafayette, Indiana, USA

[3]Department of Chemistry, Purdue University, West Lafayette, Indiana, USA

Correspondence
Sabre Kais, Department of Physics, Purdue University, West Lafayette, In 47907, USA.
Email: kais@purdue.edu

Funding information
Quantum Science Center, a National Quantum Information Science Research Center of the U.S. Department of Energy (DOE).

Abstract

Analyzing phase transitions using the inherent geometrical attributes of a system has garnered enormous interest over the past few decades. The usual candidate often used for investigation is graphene—the most celebrated material among the family of tri-coordinated graphed lattices. We show in this report that other inhabitants of the family demonstrate equally admirable structural and functional properties that at its core are controlled by their topology. Two interesting members of the family are cyclooctatrene (COT) and COT-based polymer: poly-bi-[8]-annulenylene, both in one and two dimensions that have been investigated by polymer chemists over a period of 50 years for its possible application in batteries exploiting its conducting properties. A single COT unit is demonstrated herein to exhibit topological solitons at sites of a broken bond similar to an open one-dimensional Su–Schrieffer–Heeger (SSH) chain. We observe that poly-bi-[8]-annulenylene in one dimension mimics two coupled SSH chains in the weak coupling limit, thereby showing the presence of topological edge modes. In the strong coupling limit, we investigate the different parameter values of our system for which we observe zero-energy modes. Further, the application of an external magnetic field and its effects on the band flattening of the energy bands has also been studied. In two dimensions, poly-bi-[8]-annulenylene forms a square-octagon lattice which upon breaking time-reversal symmetry goes into a topological phase forming noise-resilient edge modes. We hope our analysis would pave the way for synthesizing such topological materials and exploiting their properties for promising applications in optoelectronics, photovoltaics, and renewable energy sources.

Key Points

- We show in this paper tri-coordinated lattice systems: cylooctatrene (COT) and COT-based polymer: poly-bi-[8]-annulenylene exhibit exotic topological properties.
- Flat bands are generated upon application of tailored magnetic flux for poly-bi-[8]-annulenylene in one dimension.
- Insights from this paper open the possibility of using these polymers as an experimental ground to observe many flat-band and topology-related phenomena.

KEYWORDS
organic polymers, poly-bi-[8]-annulenylene, topological edge states, flat bands

INTRODUCTION

From the discovery of the quantum Hall effect in the 1980s,[1,2] the perception of phases in condensed matter physics underwent a foundational metamorphosis. Phase transition in such systems, formerly studied through the lens of Landau's theory of symmetry breaking,[3,4] were subsequently analyzed using abstruse yet mathematically elegant characterization of the inherent geometrical attributes of the system thereby initiating a robust bridge to topology.[5] Such interconnections have positively impacted many other domains of physics including atomic physics and quantum optics,[6–10] bioinformatics,[11–13] quantum field theory,[14] high-energy physics,[15,16] and astronomy[17,18] even though condensed matter physics indisputably continues to be the most ardent and persistent beneficiary. A quintessential example in the latter domain which has arrested enormous attention over the past several decades is the family of organic polymers like polyacetylene,[19] which possesses albeit simple yet rich topological features in one dimension[20] rooted in the Su–Schrieffer–Heeger (SSH) model.[21,22] Discovery of such polymers has revolutionized diverse applications like molecular electronics,[23–25] light-emitting diodes,[26,27] rechargeable batteries[28–30] to name a few, owing to their fascinating conducting properties usually accredited to the implicit topology and lattice geometry.

The natural extension of the aforesaid paradigm to two dimensions began with the idea of Haldane,[31] which introduces a complex second nearest neighbor hopping amplitude in graphene, which is inarguably the most widely known honeycomb lattice belonging to the larger umbrella of trivalent graphed lattices (i.e., lattice geometries with coordination number equal to 3) as shown in Figure 1. The by-product of such an endeavor is the decimation of the time-reversal symmetry (TRS) of the system thereby culminating in a natural emergence of a topological phase that is experimentally realizable.[32] Extension of the paradigm to structural chemistry has been the harbinger of a plethora of unforeseen opportunities that has duly engendered interest.[33–36] Most notably with prodigious improvements in synthetic capabilities of metal-organic, covalent-organic frameworks (MOFs/COFs)[37–42] and hydrogen-bond organic frameworks (HOFs),[43] the dream of artificially designing such polymeric substrates with tunable topological features is no longer distant. Inspired by such developments, in this work, we strive to venture beyond graphene into other members of the family of trivalent graphs which despite having the potential for offering tantalizing prospects have been severely underutilized in the literature. We focus on the Goldilocks zone of such polymers (marked in red in Figure 1) which have either been directly synthesized and shown to be excellent conductors as highlighted in a patent[44] and paper[45] or offer an easy possibility of being naturally synthesizable or artificially designed through a network of superconducting coplanar waveguides.[46] Such lattices share similar structural cohomology with the hexagonal lattice of graphene[47,48] and as we shall unravel also inherit some exotic topological features even within the framework of tight-binding (TB) approximations which form the basis to interpret all their functional attributes.

The article is structured as follows. First, we consider a single cycloctatetraene (COT) unit which forms the basic building block for poly-bi-[8]-annulenylene networks, an object of primary investigation in this work. We show how a COT unit forms topological solitons at

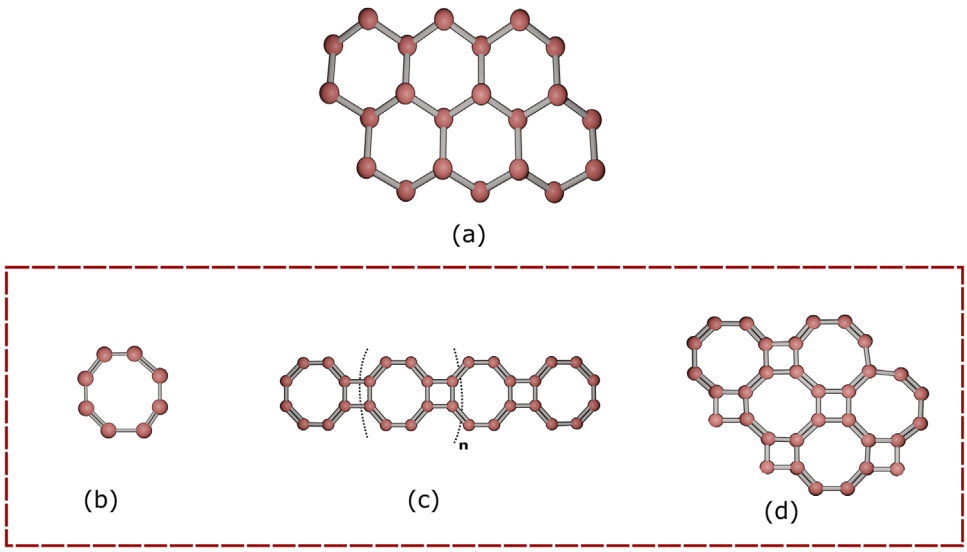

FIGURE 1 (a) Graphene, (b) cycloctatetraene (COT) unit, (c) repeating poly-bi-[8]-annulenylene in one dimension, and (d) repeating poly-bi-[8]-annulenylene in two dimensions. The red box indicates the Goldilocks zone of COT and COT-based polymers.

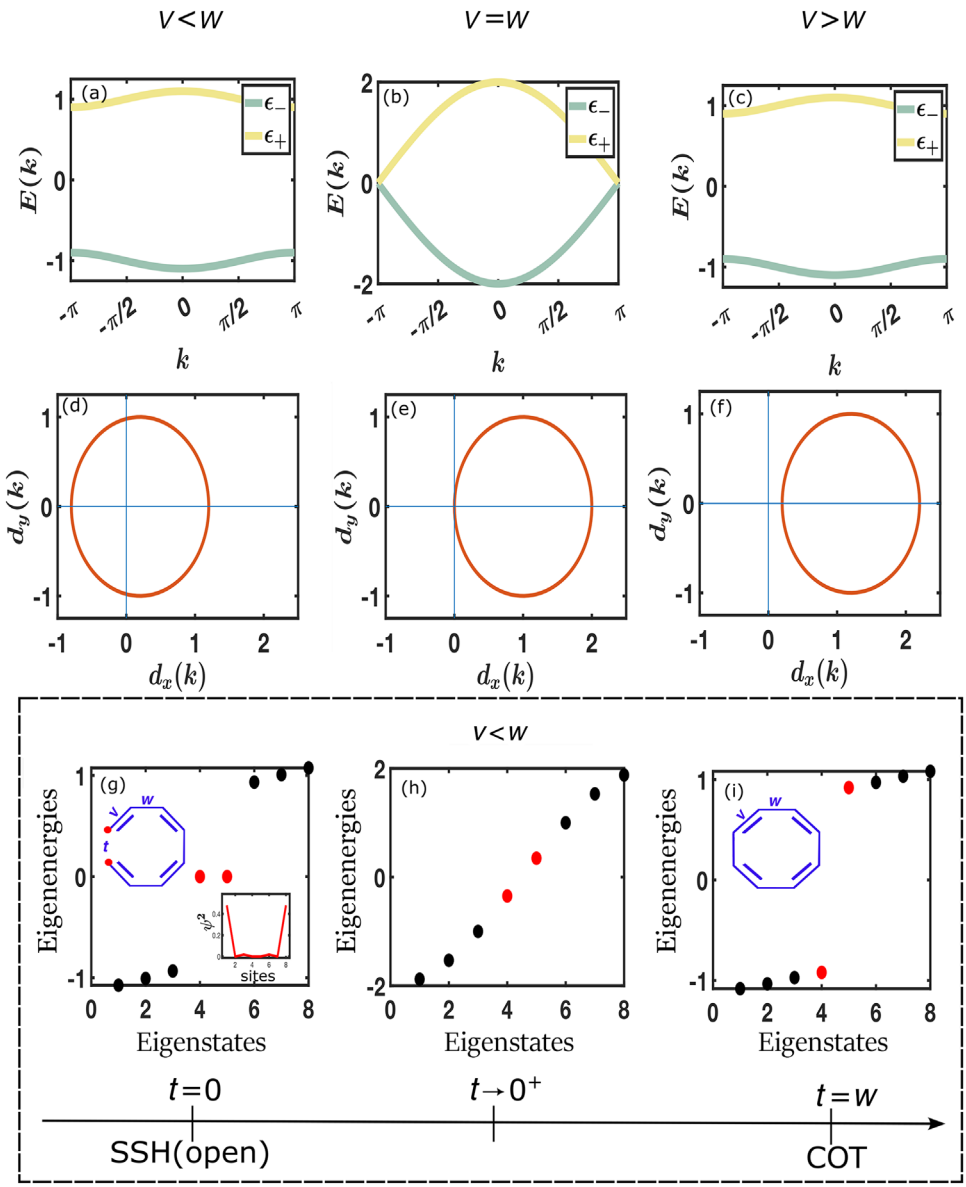

FIGURE 2 In (a)–(c), we explicate the band structure of the model described in Equations (2) and (5). (a) The spectrum ($E(k)$ vs. k) under periodic boundary conditions (PBC) in the topological phase. (b) Similar to (a) but at the critical point showing the closure of the bulk gap. (c) Similar to (a) but in the trivial phase. (d) The locus of the vector $\vec{d}_k$ (see Equation 5) in the topological phase with the origin enclosed, (e) at the critical point where the curve goes through the origin, and (f) in the trivial phase with the origin not enclosed. The energy spectrum under open boundary conditions (OBC) (g) showing the presence of edge modes in the topological phase, (h) in the bulk-conducting phase, and (i) band-insulating (topologically trivial) phase. The inset in (g) shows the electronic density distribution corresponding to the edge modes being localized at the edges of the chain.

two ends by envisioning it as a simple one-dimensional (1D) SSH chain. Then we go on to study the band structure of poly-bi-[8]-annulenylene in one dimension and unravel its inherent topological properties both in the strong and weak coupling regime. In the weak regime, we consider poly-bi-[8]-annulenylene as two weakly coupled 1D SSH chains. Following that, we further analyze the effects of band flattening of all the energy bands of 1D poly-bi-[8]annulenylene in the presence of an external magnetic field. Such band flattening can lead to localized electronic states with exotic correlated behavior. We also study the two-dimensional (2D) extension of this lattice geometry and calculate its band structure both with and without breaking TRS in order to distinguish topologically trivial and nontrivial phases. All analysis is conducted for both periodic (PBC) and open-boundary conditions (OBC) and the possibility of engineering a spin network for realizing the 2D analog is explicitly discussed.

METHODS

Calculation of winding number for COT

The winding number of the COT envisioned as an SSH chain is a topological invariant that characterizes its topological phase in one dimension. This topological invariant described by the number of times

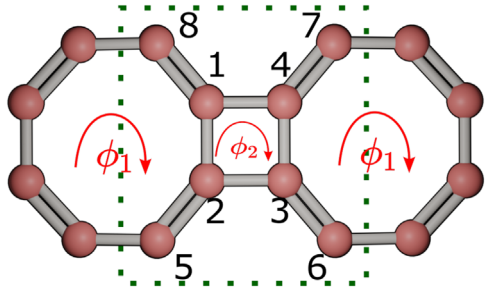

FIGURE 3 Fluxes ϕ_2 through the square and ϕ_1 through octagon plaquettes along the chosen clockwise direction. The green box shows a unit cell of poly-bi-[8]-annulenylene.

the winding vector $\vec{d}_k$ of the SSH Hamiltonian winds around the origin as shown in Figure 2d–f is given by[49]

$$\gamma = \frac{1}{2\pi}\int_{-\pi}^{\pi}\left(\vec{d}_k \times \frac{d\vec{d}_k}{dk}\right) dk = \begin{cases} 1, & |v/w| < 1 \\ 0, & |v/w| > 1 \end{cases} \tag{1}$$

Pierls substitution and flatness ratios

The Pierls substitution terms in the hopping parameters of the Hamiltonian and the flatness ratios computed to measure the flatness of the Bloch bands are discussed in this section. Considering uniform fluxes ϕ_1 and ϕ_2 through the octagon and square plaquettes as shown in Figure 3. The resulting modification in the hopping terms along the octagon plaquette,

$$e^{i\phi}[-v(c^{\dagger}_{r,4}c_{r,7}), -w(c^{\dagger}_{r,8}c_{r,7}), -v(c^{\dagger}_{r,1}c_{r,8}), -t(c^{\dagger}_{r,2}c_{r,1}),$$
$$-v(c^{\dagger}_{r,5}c_{r,2}), -w(c^{\dagger}_{r,6}c_{r,5}), -v(c^{\dagger}_{r,3}c_{r,6}), -t(c^{\dagger}_{r,4}c_{r,3})]$$

and along the square plaquette,

$$e^{i\phi}[-w(c^{\dagger}_{r,4}c_{r,1}), -t(c^{\dagger}_{r,3}c_{r,4}), -w(c^{\dagger}_{r,2}c_{r,3}), -t(c^{\dagger}_{r,1}c_{r,2})]$$

and their Hermitian-conjugate (*h.c*) parts.

The flatness ratio $g = E_{bw}/\Delta$,[50–52] where E_{bw} is the bandwidth and Δ is the bandgap is defined for the VB and CB. For all other bands, we consider the ratio $h = \langle V_F\rangle_K^{-(+)}/\langle V_F\rangle_K^{VB(CB)}$, where $\langle V_F\rangle_K$ denotes Fermi

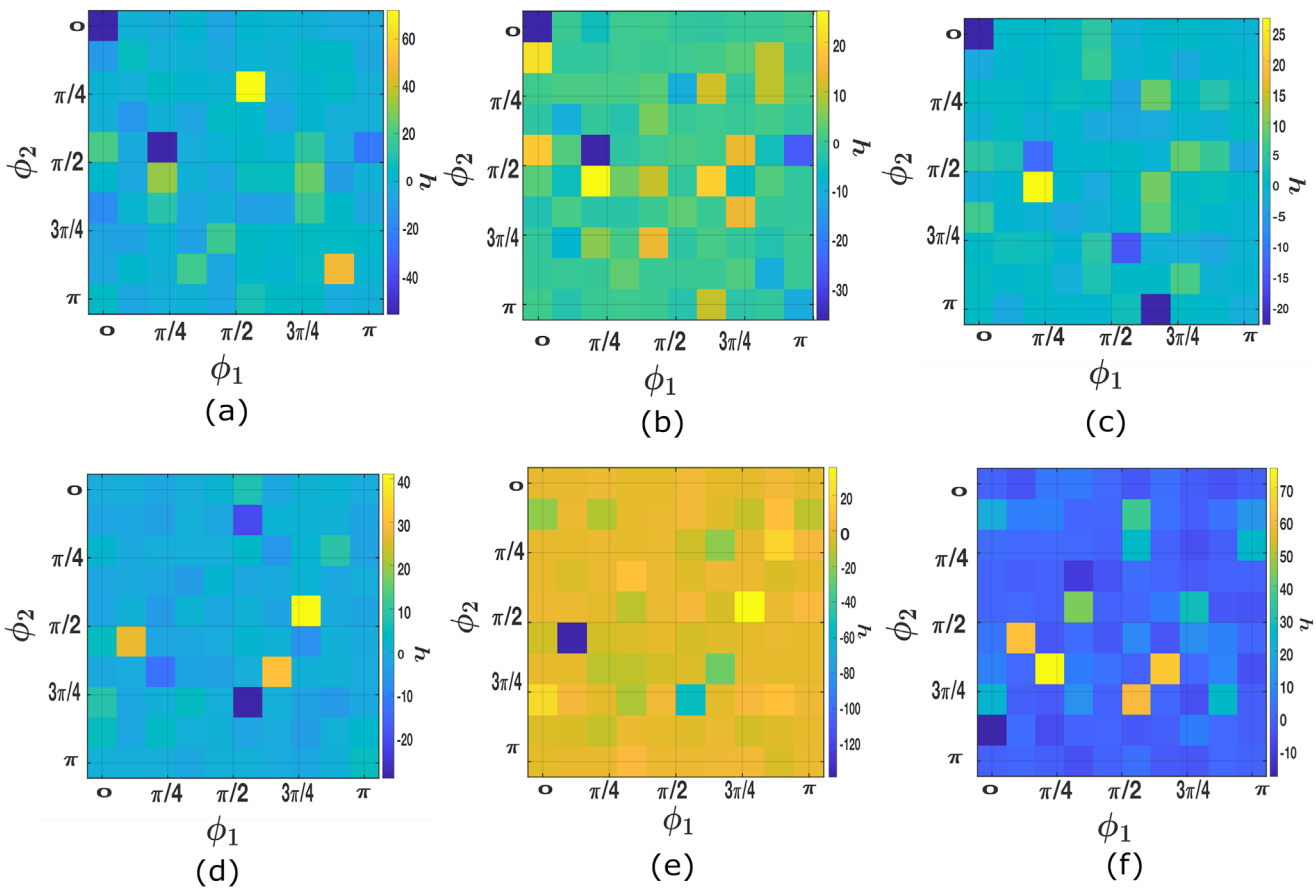

FIGURE 4 Color-coded plot of (a)–(c) Flatness ratio *h* for the negative energy bands. (d)–(f) Flatness ratio *h* for the positive energy bands in (ϕ_1, ϕ_2) plane for $v = w = t = 1$.

Natural Sciences

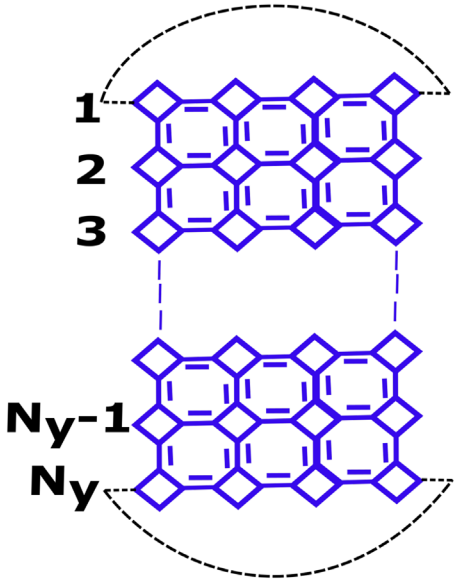

FIGURE 5 Schematic of a cylindrical strip with PBC along the x-direction and OBC along the y-direction. N_y denotes the finite number of unit cells considered along the y-direction.

velocity averaged over the entire Brillouin Zone and −(+) denotes negative (positive) energy Bloch bands of the concerned system. The corresponding color-coded plots for the other bands are shown in Figure 4.

Tight-binding: Finite size calculations

To study finite-size effects, we consider quasi-OBC, that is, the open boundary condition along y keep the periodicity intact along x as shown in Figure 5. This forms a cylindrical strip with a finite number of cells in the y-direction alone thus forming zig-zag edges as shown.

For instance, for $N_y = 4$ unit cells, the quasi-OBC Hamiltonian of poly-bi-[8]-annulenylene in two dimensions has the following form:

$$\begin{pmatrix} 0 & we^{-i\phi} & 0 & te^{-i\phi} & 0 & 0 & 0 & 0 \\ we^{i\phi} & 0 & te^{-i\phi} & ve^{ik_x}e^{-i\phi} & 0 & 0 & 0 & 0 \\ 0 & te^{i\phi} & 0 & we^{-i\phi} & ve^{-i\phi} & 0 & 0 & 0 \\ te^{i\phi} & ve^{-ik_x}e^{i\phi} & 0 & we^{i\phi} & 0 & 0 & 0 & 0 \\ 0 & 0 & ve^{i\phi} & 0 & 0 & we^{-i\phi} & 0 & te^{-i\phi} \\ 0 & 0 & 0 & 0 & we^{i\phi} & 0 & te^{-i\phi} & ve^{ik_x}e^{-i\phi} \\ 0 & 0 & 0 & 0 & 0 & te^{i\phi} & 0 & we^{-i\phi} \\ 0 & 0 & 0 & 0 & te^{i\phi} & ve^{i\phi}e^{-ik_x} & we^{i\phi} & 0 \end{pmatrix}.$$

RESULTS AND DISCUSSION

Cycloctatetraene as a SSH chain

To explore the topology of COT, we begin by considering a single COT unit as a closed and periodic SSH chain. The well-known SSH chain

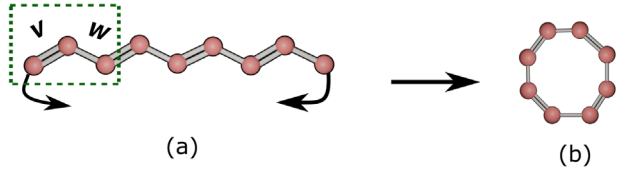

FIGURE 6 (a) 1D SSH chain (a unit cell encompassed in the green box). (b) COT as a closed SSH chain.

offers a paradigmatic example of supporting a 1D topological insulating phase. The Hamiltonian of the model is as follows[21]

$$H_{SSH} = -v\sum_{i=1}^{N} c_{2i-1}^{\dagger}c_{2i} - w\sum_{i=1}^{N} c_{2i}^{\dagger}c_{2i+1} + h.c \tag{2}$$

where v, w are the alternating hopping strengths, N denotes the number of unit cells with a single unit cell marked in green as shown in Figure 6a $c^{\dagger}$, c denotes the creation and annihilation operators describing an electron hopping in a lattice between sites designated as i, and $h.c$ denote Hermitian conjugate.

The Hamiltonian can be diagonalized through a Fourier transformation,[53,54]

$$H_{SSH} = -\sum_{k} \psi_k^{\dagger} H_k \psi_k = -\sum_{k} \psi_k^{\dagger}(\vec{d}_k.\vec{\sigma})\psi_k \tag{3}$$

where $k * a_0 \in [-\pi, \pi]$ denotes a discrete set of points over the Brillouin zone in reciprocal space with a_0 being the real space lattice separation. $(\psi_k^{\dagger}, \psi_k)$ and H_k denote Bloch vectors and Hamiltonian in the reciprocal space, respectively. The $\vec{d}_k$ and the energy of the bands are expressed as

$$\vec{d}_k = (v + w\cos(kx), w\sin(kx), 0) \tag{4}$$

$$\epsilon_{\pm} = \sqrt{d_x^2 + d_y^2} = \pm\sqrt{v^2 + w^2 + 2vw\cos(k)} \tag{5}$$

As shown in Figure 2, We have the trivial insulator phase for $v > w$, the metallic phase for $v = w$, and the topological insulator phase for $v < w$. The topological phase is further characterized by the nonzero winding number[49] (see the Methods section for calculation of winding number) and the appearance of edge states.

Poly-bi-[8]-annulenylene in one dimension

For poly-bi-[8]-annulenylene, the unit cell marked in green in Figure 7, has eight sites. The Hamiltonian of the model is as follows:

$$\begin{aligned} H_{PO[8]A} = \sum_{r=1}^{N}[&-v(c_{r,1}^{\dagger}c_{r,8} + c_{r,4}^{\dagger}c_{r,7} \\ &+ c_{r,2}^{\dagger}c_{r,5}) - w(c_{r,1}^{\dagger}c_{r,4} + c_{r,2}^{\dagger}c_{r,3}) \\ &- t(c_{r,1}^{\dagger}c_{r,2} + c_{r,4}^{\dagger}c_{r,3})] + h.c, \end{aligned} \tag{6}$$

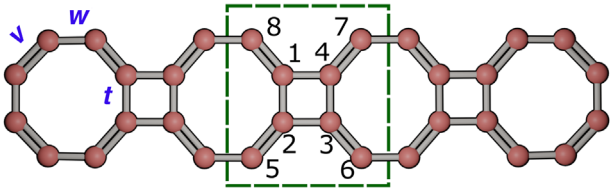

FIGURE 7 Poly-bi-[8]-annulenylene moiety with the chosen unit cell shown inside the rectangular box. *v*, *w*, and *t* shown are the respective hopping parameters.

where *v*, *w*, and *t* are the respective hopping strengths between different lattice sites in a unit cell as shown in Figure 7. The subscript *r*, *i* contains $i = 1..8$ going over all the eight sites in a unit cell and *r* going over *N* number of unit cells. Following a Fourier transformation, we solve the *k*-space Hamiltonian with the following form:

$$H_{PO[8]A} = -\sum_k \psi_k^\dagger [H(k)_{8\times 8}]\psi_k. \tag{7}$$

The corresponding band structure has eight bands as shown in Figure 8a. Among the eight bands, we focus on the valence and conduction band (marked as VB and CB) around the Fermi level (i.e., $E(k) = 0$ level). We focus on two cases. *Weak coupling*: When the coupling strength $t << v$ and $t << w$, one can envision the lattice of poly-bi-[8]-annulenylene as two weakly coupled SSH chains[55,56] as shown in Figure 7b with parameter *t* playing the role of linking between two chains.

In Figure 8, we show the band structure of the model defined in Equation (6) focusing exclusively on the energy bands close to the Fermi level in both the trivial and topological phase under PBC (Figure 8b,c) and OBC (Figure 8d,e). In the topological phase under OBC, we expect four edge states corresponding to four edges of two weakly coupled SSH chains. This is further corroborated through numerical evidence in Figure 8e. Further, the resilience of these modes against noise has been discussed in the Supporting Information. This observation can be generalized to *N* weakly coupled SSH chains wherein 2*N* edge modes would be encountered.

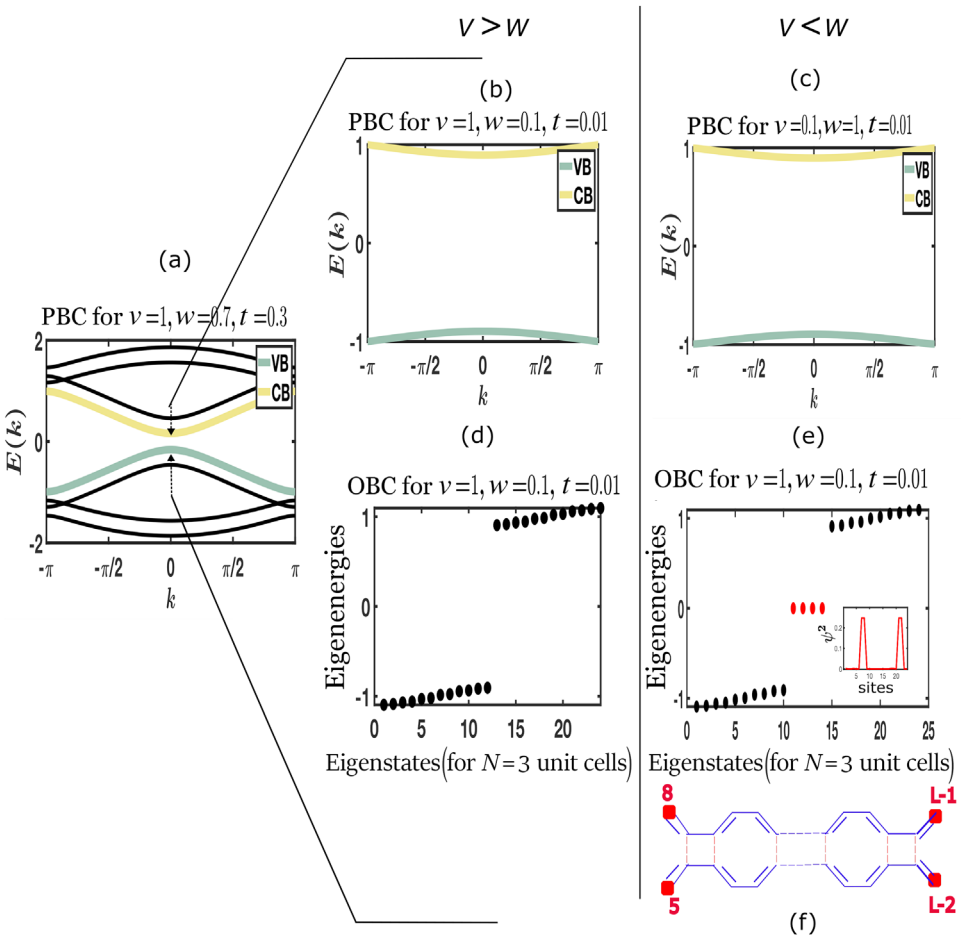

FIGURE 8 (a) Band structure of poly-bi-[8]-annulenylene with $v = w = 1$, $t = 0.1$ highlighting the behavior of two weakly coupled SSH chains under PBC. (b) The spectrum as in (a) but computed in the trivial phase ($v > w$). (c) The spectrum as in (a) but computed in the topological phase ($v < w$). All plots are generated in the weakly coupled regime as defined by $t << w$ and $t << v$. (d) The energy spectrum under OBC shows the absence of edge modes at zero energy in the trivial phase. (e) Similar spectrum as in (d) but showing the presence of edge modes at zero energy in the topological phase. The inset shows electronic density distribution of the edge modes being localized at the four edges of a finite poly-bi-[8]-annulenylene. (f) Four edges of a finite poly-bi-[8]-annulenylene.

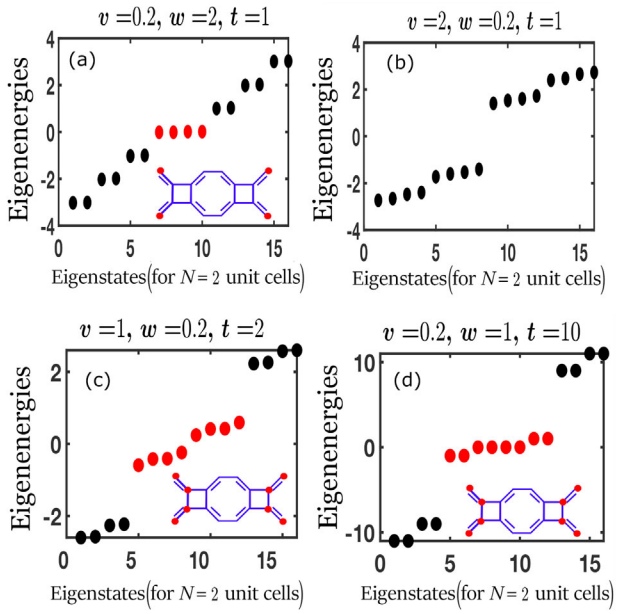

FIGURE 9 (a)–(d) The energy spectrum with open boundary conditions showing the absence and presence of zero modes in different parameter regimes. The insets in (a)–(c) show eight edges of a finite poly-bi-[8]-annulenylene for $N = 2$ unit cells.

Strong coupling: When the coupling is strong, the two stacked chains form dimers in several ways. Several such cases have been shown in Figure 9. All such cases are constructed under OBC and show the relative displacement in the energy spectrum of the eight edge states (see Figure 9b,d) under different parameter choices. In general for N such strongly coupled chains, one can prepare a maximum of $8N$ such edge states in the topological phase.

Magnetix flux through 1D poly-bi-[8]-annulenylene

In this section, we study how the flatness of the Bloch bands could be tuned by magnetic fluxes through the square and octagon plaquettes of poly-bi-[8]-annuleneylene. In the presence of an external magnetic field, the wave function of a charged particle going around a closed loop acquires an Aharonov–Bohm phase shifts proportional to the magnetic flux through the enclosed loop.[57] In the TB language, this phase gets reflected in the electron hopping amplitudes modified with an acquired extra phase factor given by the Pierls substitution,[58]

$$T_{ij} \to T_{ij} e^{\pm i\phi}, \tag{8}$$

where T_{ij} is the hopping amplitude between sites i and j. For convention, we take positive flux in the clockwise direction and vice versa.

We consider fluxes ϕ_1 and ϕ_2 impinging the octagon and square plaquettes as in Figure 3. Adopting this sort of general and nonunique flux profile thus allowing even small to large fluctuations (i.e., $\phi_1 \neq \phi_2$ always) in the fluxes penetrating octagon and square plaquettes owing to the fact that these two plaquettes have different geometries enables us to explore the flatness of these bands across a 2D parameter space. We plot the flatness ratios defined in the Methods section of valence and conduction bands in the (ϕ_1, ϕ_2) plane as shown in Figure 10. Flatness ratios and their plots of other bands in the (ϕ_1, ϕ_2) plane are presented in the Methods section.

We observe that all energy bands display considerable flatness (according to the used metric defined in the Methods section), hence can admit small Fermi velocity of an initialized electronic wavepacket leading to nontrivial consequences. Recently, such flat bands are being routinely investigated in twisted bilayer graphene[59–61] wherein Moire superlattices are formed at a wavelength scale much bigger than the atomic separation in graphene. In these superlattices, hybridization of the energy bands from the two layers leads to flat bands when the twist angle is very low similar to what we see here. Such bands have localized electronic density and can be the hotbed for studying many correlated Fermionic behavior as has been seen in a correlated Mott insulator under moderate occupancy[62–65] or even a superconducting phase at low occupancy.[63,66,67] Another potential correlated phenomenon that can be realized in poly-bi-[8]-annulenylene is the exciton condensation which has been recently predicted in a highly amorphous nickel tetrathiafulvalene-tetrathiolate polymer.[68] Particular emphasis should be given to the proposed polymer: poly-bi-[8]-annulenylene, as this polymer could serve as a platform to undertake various studies involving the interplay of topology, flat bands, and exciton condensation phenomena. This is beyond the scope of the present study; we leave it for a future study where one can consider calculations of particle-hole reduced density matrix (RDM) and look for signatures[69] of exciton condensation phenomena by adopting advanced electronic structure techniques like variational 2-RDM .[70,71] Even though we have described the electronic states only, the coupling of the Bloch states of the flat bands with spin can lead to many exotic spin–orbit interaction schemes like in Dzyaloshinskii–Moriya scheme[72–74] and ferromagnetic Mott state.[75] A subset of these phenomena has been extended to transition-metal dichalcogenides[76,77] too, and there is no apparent reason why poly-bi-[8]-annulenylene lattice cannot be the next fascinating test bed. In fact, it must be emphasized that unlike in the graphene bilayer where mechanical twisting is necessary, herein we are able to generate flat bands under modest conditions using just a single chain with an experimentally tailored magnetic flux profile. Additionally, if one of the fluxes is small compared to the other (for instance, $\phi_2 \to 0$ and $\phi_1 \neq 0$), that still leads to considerable flatness of the aforementioned bands as shown in Figure 10.

Poly-bi-[8]-annulenylene in two dimensions

The 2D lattice of poly-bi-[8]-annulenylene has repeated COT units in both the x and y directions connected by squares. This lattice geometry has squares and octagons as its fundamental plaquettes. We investigate the lattice cleaved at 45 as it reduces the lattice to a square with only four sites per unit cell, marked in red in Figure 11a. The lattice vectors in Figure 11a are $\vec{a}_1 = (1, 0)$ and $\vec{a}_2 = (0, 1)$ with the

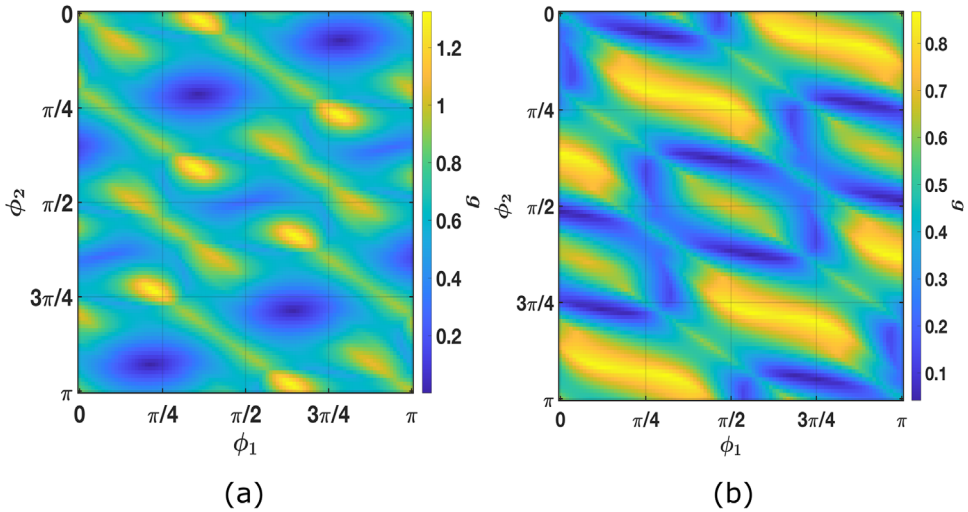

FIGURE 10 Color-coded plot of (a) flatness ratio g for the valence band and (b) flatness ratio g for the conduction band in (ϕ_1, ϕ_2) plane for $v = w = t = 1$.

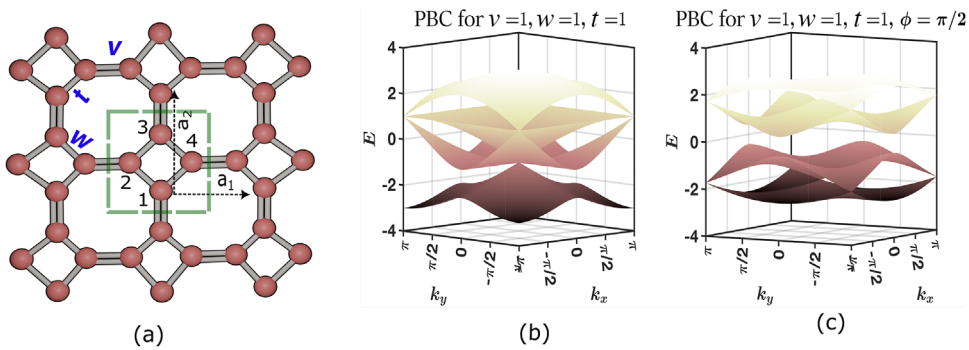

FIGURE 11 (a) Square-octagon lattice of poly-bi-[8]-annulenylene in two dimensions with the unit cell containing four sites boxed. (b) Band structure with $v = w = t = 1$. (c) Band structure with $v = 2, w = 1, t = 1, \phi = \pi/2$ as described by the new Hamiltonian equation (10).

lattice constant taken to be unity. The Hamiltonian in the reciprocal space is given by

$$H(k) = \begin{pmatrix} 0 & w & ve^{-ik_y} & t \\ w & 0 & t & ve^{ik_x} \\ ve^{ik_y} & t & 0 & w \\ t & ve^{-ik_x} & w & 0 \end{pmatrix}, \tag{9}$$

where v, w, and t are nearest neighbor hopping amplitudes as shown in Figure 11a. Figure 11b shows the band structure of the model defined in Equation (9) under PBC. Since the unit cell has four sites, there are four bands in the said figure.

Our primary motivation is to explore the topological properties of the lattice and study what conditions lead to the emergence of zero-energy edge modes. To this end, we adopt the same technique as discussed in Haldane,[31] which involves raising the time-reversal invariance thereby culminating in band opening at time-reversal invariant momenta points (Γ and K).[78] This is akin to introducing a complex hopping parameter for nearest neighboring interactions such that the resulting Hamiltonian has the following form:

$$\begin{pmatrix} 0 & we^{-i\phi} & ve^{-ik_y}e^{-i\phi} & te^{-i\phi} \\ w & 0 & te^{-i\phi} & ve^{ik_x}e^{i\phi} \\ ve^{ik_y}e^{i\phi} & te^{i\phi} & 0 & we^{-i\phi} \\ te^{i\phi} & ve^{-ik_x}e^{i\phi} & w & 0 \end{pmatrix}, \tag{10}$$

where $e^{i\phi}$ is the complex hopping term introduced. In Figure 11c, we show the resultant band structure of the model defined in Equation (10) wherein band opening as discussed above is clearly evidential.

To envision the edge modes, it is sufficient to consider quasi-OBC, that is, periodicity in the x-direction and aperiodicity in the y-direction thus forming a cylindrical strip as explained in the Methods section. We show the appearance of zero-energy eigenmodes corresponding to this type of edge in the eigenspectrum (Figure 12b, marked in red). We observe that such edge modes only occur in the topological phase for particular values of the parameters of the Hamiltonian after breaking the time-reversal symmetry of our system with complex coupling terms thereby indicating the formation of topological edge modes.

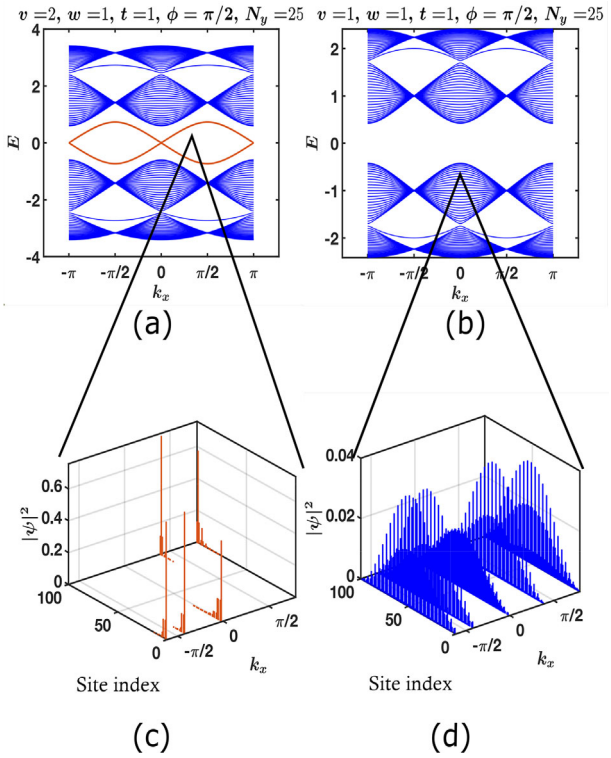

FIGURE 12 (a) Spectrum of OBC along the y-the direction and PBC in the x-direction. Marked in red: edge modes. (b) Spectrum of OBC along the y-the direction and PBC in the x-direction. Marked in red: edge modes. (c) Electron density distribution of edge mode excitation. (d) Electron density distribution of a bulk mode. N_y denotes the number of finite unit cells taken along the y-direction.

CONCLUSION

We have studied the topology of COT and its associated polymeric structure: poly-bi-[8]-annulenelene. We have presented ways to construct a number of topological excitations, that is, zero-energy edge modes both in strong as well as weak coupling regimes. By realizing the fact that the application of an external magnetic field affects the flatness of the bands, we have constructed systematic ways to tune the flatness of all the bands with uniform fluxes through every plaquette of the lattice geometry of 1D poly-bi-[8]-annulenylene. The 2D extension of these polymers has Dirac points (similar to graphene) and also supports topological phases upon lifting the time-reversal symmetry. The resilience of the incipient edge modes against noise has been discussed extensively (see the Supporting Information). The discussed structures not only show promising conducting properties making them fundamental candidates for the Li/Na-ion batteries[44,45,79] but also as we have shown in this article possess inherent topological characteristics and flatbands in the presence of an external magnetic field. Such insights are crucial to understanding its conducting properties and open the possibility of using these polymers as an alternative experimental ground to observe many flat-band-related phenomena as opposed to the previously used MOF/COF- and HOF-based platforms.

Another interesting avenue which may benefit from a more careful investigation (to be undertaken shortly) is the prospect of simulating the physical effects studied in this article on quantum hardware. With the recent advent of engineering lattices with superconducting qubits/cold atoms, COT- and COT-based polymers could be engineered on table-top experiments and further exploited for their rich topological properties not only within a spinless Fermionic model but can also be realized using a spin graph phase as has been discussed explicitly in the first section of the Supporting Information. In fact, hybrid quantum simulation of materials and molecules and other physical systems have already begun to gain attention with interesting possibilities being explored[80–85] including harnessing exotic correlation like entanglement.[86] Taking a step further, we show in this article that an engineered spin Hamiltonian, that is, a Kitaev spin liquid is capable of generating the same interaction as illustrated in Equation (10) after Jordan–Wigner transformation and majoranization. This opens up a lot of possibilities for direct experimental simulation of the 2D lattice on superconducting hardware or even a cold-atom-based quantum simulator.[87,88] In short, we have just scratched the surface. The scope of possibilities to develop poly-bi-[8]-annulenylene (in both one and two dimensions) as the next prospective candidate for beneficial applications as well as for procuring fundamental theoretical insight is practically endless. The authors hope that the findings in this article will duly bring into limelight other members of the tri-coordinated graphed lattices to unravel the unforeseen and untapped chemistry these candidates are capable of displaying.

AUTHOR CONTRIBUTIONS

Varadharajan Muruganandam: Data curation (lead), formal analysis (equal), investigation (lead), writing - original draft (lead). Manas Sajjan: Conceptualization (equal), data curation (supporting), formal analysis (equal), investigation (supporting), methodology (lead), validation (equal), writing - original draft (supporting). Sabre Kais: Conceptualization (lead), funding acquisition (lead), project administration (lead), supervision (lead), validation (equal), writing - original draft (supporting).

ACKNOWLEDGMENTS

We thank Prof. Xingshan Cui from the Department of Mathematics, Purdue University for many useful discussions. The authors would like to acknowledge the financial support from the Quantum Science Center, a National Quantum Information Science Research Center of the U.S. Department of Energy (DOE).

CONFLICT OF INTEREST STATEMENT

The authors declare no conflicts of interest.

DATA AVAILABILITY STATEMENT

All data used to support the findings of the study will be available with the corresponding author upon reasonable request.

ETHICS STATEMENT

The authors confirm that they have followed the ethical policies of the journal.

ORCID

Varadharajan Muruganandam https://orcid.org/0000-0001-7888-2603

Sabre Kais https://orcid.org/0000-0003-0574-5346

PEER REVIEW

The peer review history for this article is available at https://publons.com/publon/10.1002/ntls.20230015.

REFERENCES

1. Klitzing Kv, Dorda G, Pepper M. New method for high-accuracy determination of the fine-structure constant based on quantized Hall resistance. *Phys Rev Lett*. 1980;45:494-497.
2. Tsui DC, Stormer HL, Gossard AC. Two-dimensional magnetotransport in the extreme quantum limit. *Phys Rev Lett*. 1982;48:1559-1562.
3. Ter Haar D. *Collected Papers of LD Landau*. Elsevier; 2013.
4. Hoffmann KH, Tang Q. *Ginzburg-Landau Phase Transition Theory and Superconductivity*. International Series of Numerical Mathematics, Vol 134. Birkhäuser; 2012.
5. Bredon GE. *Topology and Geometry*. Graduate Texts in Mathematics, Vol 139. Springer Science & Business Media; 2013.
6. Diehl S, Rico E, Baranov MA, Zoller P. Topology by dissipation in atomic quantum wires. *Nat Phys*. 2011;7:971-977.
7. Perczel J, Borregaard J, Chang DE, et al. Topological quantum optics in two-dimensional atomic arrays. *Phys Rev Lett*. 2017;119:023 603.
8. Barik S, Karasahin A, Flower C, et al. A topological quantum optics interface. *Science*. 2018;359:666-668.
9. Amo A. When quantum optics meets topology. *Science*. 2018;359:638-639.
10. Barik S, Karasahin A, Mittal S, Waks E, Hafezi M. Chiral quantum optics using a topological resonator. *Phys Rev B*. 2020;101:205 303.
11. Adams C, Devadoss J, Elhamdadi M, Mashaghi A. Knot theory for proteins: Gauss codes, quandles and bondles. *J Math Chem*. 2020;58:1711-1736.
12. Mishra R, Bhushan S. Knot theory in understanding proteins. *J Math Biol*. 2012;65:1187-1213.
13. Sułkowska JI, Sułkowski P, Onuchic J. Dodging the crisis of folding proteins with knots. *Proc Natl Acad Sci*. 2009;106:3119-3124.
14. Witten E. Topological quantum field theory. *Commun Math Phys*. 1988;117:353-386.
15. Donnelly W, Jiang Y, Kim M, Wong G. Entanglement entropy and edge modes in topological string theory. Part I. Generalized entropy for closed strings. *J High Energy Phys*. 2021;2021:1-64.
16. Cole A, Shiu G. Topological data analysis for the string landscape. *J High Energy Phys*. 2019;2019:1-31.
17. Wei SW, Liu YX, Mann RB. Intrinsic curvature and topology of shadows in Kerr spacetime. *Phys Rev D*. 2019;99:041 303.
18. Wei SW. Topological charge and black hole photon spheres. *Phys Rev D*. 2020;102:064 039.
19. Shirakawa H, McDiarmid A, Heeger A. Focus article: twenty-five years of conducting polymers. *Chem Commun*. 2003;2:1-4.
20. Meier EJ, An FA, Gadway B. Observation of the topological soliton state in the Su–Schrieffer–Heeger model. *Nat Commun*. 2016;7:13986. https://doi.org/10.1038/ncomms13986
21. Su WP, Schrieffer JR, Heeger AJ. Solitons in polyacetylene. *Phys Rev Lett*. 1979;42:1698-1701.
22. Nobelprize.org. *The Nobel Prize in Chemistry 2000*. 2000. https://www.nobelprize.org/prizes/chemistry/2000/press-release
23. Lakshmi S, Dutta S, Pati SK. Molecular electronics: effect of external electric field. *J Phys Chem C*. 2008;112:14 718-14 730.
24. Jean N, Sanvito S. Inelastic transport in molecular spin valves: calculations using the tight-binding Su-Schrieffer-Heeger model. *Phys Rev B*. 2006;73:094 433.
25. Ness H, Fisher A. Vibrational inelastic scattering effects in molecular electronics. *Proc Natl Acad Sci*. 2005;102:8826-8831.
26. Johansson A, Stafström S. Polaron dynamics in a system of coupled conjugated polymer chains. *Phys Rev Lett*. 2001;86:3602-3605.
27. Meng Y, Liu X, Di B, An Z. Recombination of polaron and exciton in conjugated polymers. *J Chem Phys*. 2009;131:244 502.
28. Xie Z, Kang Ym, An Z, Li Yc. Two-dimensional localized vibrational modes of polythiophene around a bipolaron. *Phys Rev B*. 2000;61:1096-1100.
29. Goto H, Yoneyama H, Togashi F, et al. Preparation of conducting polymers by electrochemical methods and demonstration of a polymer battery. *J Chem Educ*. 2008;85:1067.
30. Heeger AJ. Semiconducting and metallic polymers: The fourth generation of polymeric materials. *J Phys Chem B*. 2001;105(36):8475-8491.
31. Haldane FDM. Model for a quantum Hall effect without Landau levels: condensed-matter realization of the "parity anomaly". *Phys Rev Lett*. 1988;61:2015-2018.
32. Jotzu G, Messer M, Desbuquois R, et al. Experimental realization of the topological Haldane model with ultracold Fermions. *Nature*. 2014;515:237-240.
33. Chakraborty G, Park IH, Medishetty R, Vittal JJ. Two-dimensional metal-organic framework materials: synthesis, structures, properties and applications. *Chem Rev*. 2021;121:3751-3891.
34. Jiang W, Ni X, Liu F. Exotic topological bands and quantum states in metal-organic and covalent-organic frameworks. *Acc Chem Res*. 2021;54:416-426.
35. Gao Z, Gao Y, Hua M, Liu J, Huang L, Lin N. Design and synthesis of a single-layer ferromagnetic metal-organic framework with topological nontrivial gaps. *J Phys Chem C*. 2020;124:27 017-27 023.
36. Jiang W, Zhang S, Wang Z, Liu F, Low T. Topological band engineering of Lieb lattice in phthalocyanine-based metal-organic frameworks. *Nano Lett*. 2020;20:1959-1966.
37. Kambe T, Sakamoto R, Hoshiko K, et al. π-Conjugated nickel bis(dithiolene) complex nanosheet. *J Am Chem Soc*. 2013;135:2462-2465.
38. Sheberla D, Sun L, Blood-Forsythe MA, et al. High electrical conductivity in Ni_3(2,3,6,7,10,11-hexaiminotriphenylene)$_2$, a semiconducting metal–organic graphene analogue. *J Am Chem Soc*. 2014;136:8859-8862.
39. Chen H, Zhang S, Jiang W, et al. Prediction of two-dimensional nodal-line semimetals in a carbon nitride covalent network. *J Mater Chem A*. 2018;6:11 252-11 259.
40. Wang ZF, Su N, Liu F. Prediction of a two-dimensional organic topological insulator. *Nano Lett*. 2013;13:2842-2845.
41. Wang Z, Liu Z, Liu F. Organic topological insulators in organometallic lattices. *Nat Commun*. 2013;4:2451. https://doi.org/10.1038/ncomms2451
42. Su N, Jiang W, Wang Z, Liu F. Prediction of large gap flat Chern band in a two-dimensional metal-organic framework. *Appl Phys Lett*. 2018;112:033 301.
43. Pan M, Zhang X, Zhou Y, et al. Growth of mesoscale ordered two-dimensional hydrogen-bond organic framework with the observation of flat band. *Phys Rev Lett*. 2023;130:036 203.
44. Cheryl D, Stevenson JPD. *Cyclooctatetraene-based cathode for electrochemical cells*. 2010. US Patent US20100288628A1.
45. Zhao X, Qiu W, Ma C, et al. Superposed redox chemistry of fused carbon rings in cyclooctatetraene-based organic molecules for high-voltage and high-capacity cathodes. *ACS Appl Mater Interfaces*. 2018;10:2496-2503.
46. Kollár AJ, Fitzpatrick M, Sarnak P, Houck AA. Line-graph lattices: Euclidean and non-Euclidean flat bands, and implementations in circuit quantum electrodynamics. *Commun Math Phys*. 2020;376:1909-1956. https://doi.org/10.1007/s00220-019-03645-8
47. Martinez J. Archimedean lattices. *Algebra Universalis*. 1973;3:247-260.

48. Chavey D. Tilings by regular polygons–II: a catalog of tilings. *Symmetry*. 1989;2:147-165.
49. Asbóth JK, Oroszlány L, Pályi A. *A Short Course on Topological Insulators*. Springer International Publishing; 2016.
50. Sun K, Gu Z, Katsura H, Das Sarma S . Nearly flatbands with nontrivial topology. *Phys Rev Lett*. 2011;106:236 803.
51. Neupert T, Santos L, Chamon C, Mudry C. Fractional quantum Hall states at zero magnetic field. *Phys Rev Lett*. 2011;106:236 804.
52. Tang E, Mei JW, Wen XG. High-temperature fractional quantum Hall states. *Phys Rev Lett*. 2011;106:236 802.
53. Bloch F. Über die quantenmechanik der elektronen in kristallgittern. *Z Phys*. 1929;52:555-600.
54. Ashcroft N, Mermin N, Mermin N. *Solid State Physics*. HRW international editions. Holt, Rinehart and Winston; 1976.
55. Li C, Lin S, Zhang G, Song Z. Topological nodal points in two coupled Su-Schrieffer-Heeger chains. *Phys Rev B*. 2017;96:125 418.
56. Padavić K, Hegde SS, DeGottardi W, Vishveshwara S. Topological phases, edge modes, and the Hofstadter butterfly in coupled Su-Schrieffer-Heeger systems. *Phys Rev B*. 2018;98:024 205.
57. Aharonov Y, Bohm D. Significance of electromagnetic potentials in the quantum theory. *Phys Rev*. 1959;115:485-491.
58. Peierls R. Zur Theorie des Diamagnetismus von Leitungselektronen. *Z Phys*. 1933;80:763-791.
59. Lisi S, Lu X, Benschop T, et al. Observation of flat bands in twisted bilayer graphene. *Nat Phys*. 2021;17:189-193.
60. Marchenko D, Evtushinsky D, Golias E, Varykhalov A, Seyller T, Rader O. Extremely flat band in bilayer graphene. *Sci Adv*. 2018;4:eaau0059.
61. Morell ES, Correa J, Vargas P, Pacheco M, Barticevic Z. Flat bands in slightly twisted bilayer graphene: Tight-binding calculations. *Phys Rev B*. 2010;82:121 407.
62. Po HC, Zou L, Vishwanath A, Senthil T. Origin of Mott insulating behavior and superconductivity in twisted bilayer graphene. *Phys Rev X*. 2018;8:031 089.
63. Yankowitz M, Chen S, Polshyn H, et al. Tuning superconductivity in twisted bilayer graphene. *Science*. 2019;363:1059-1064.
64. Choi Y, Kemmer J, Peng Y, et al. Electronic correlations in twisted bilayer graphene near the magic angle. *Nat Phys*. 2019;15:1174-1180.
65. Saito Y, Ge J, Watanabe K, Taniguchi T, Young AF. Independent superconductors and correlated insulators in twisted bilayer graphene. *Nat Phys*. 2020;16:926-930.
66. Codecido E, Wang Q, Koester R, et al. Correlated insulating and superconducting states in twisted bilayer graphene below the magic angle. *Sci Adv*. 2019;5:eaaw9770.
67. Lu X, Stepanov P, Yang W, et al. Superconductors, orbital magnets and correlated states in magic-angle bilayer graphene. *Nature*. 2019;574:653-657.
68. Schouten AO, Klevens JE, Sager-Smith LM, Xie J, Anderson JS, Mazziotti DA. Potential for exciton condensation in a highly conductive amorphous polymer. *Phys Rev Mater*. 2023;7:045 001.
69. Safaei S, Mazziotti DA. Quantum signature of exciton condensation. *Phys Rev B*. 2018;98:045 122.
70. Mazziotti D. (Ed.). *Two-Electron Reduced-Density-Matrix Mechanics: With Application to Many-Electron Atoms and Molecules*. Wiley; 2010. https://doi.org/10.1002/0470106603
71. Verstichel B, van Aggelen H, Poelmans W, Van Neck D. Variational two-particle density matrix calculation for the Hubbard model below half filling using spin-adapted lifting conditions. *Phys Rev Lett*. 2012;108:213 001.
72. Côté R, Lambert J, Barlas Y, MacDonald A. Orbital order in bilayer graphene at filling factor ν=- 1. *Phys Rev B*. 2010;82:035 445.
73. Ding C, Zhang X, Gao H, Ma X, Li Y, Zhao M. Role of electron-electron interaction in the plasmon modes of twisted bilayer graphene. *Phys Rev B*. 2022;106:155 402.
74. Li YH, Cheng R. Moiré magnons in twisted bilayer magnets with collinear order. *Phys Rev B*. 2020;102:094 404.
75. Seo K, Kotov VN, Uchoa B. Ferromagnetic Mott state in twisted graphene bilayers at the magic angle. *Phys Rev Lett*. 2019;122:246 402.
76. Pan H, Wu F, Sarma SD. Band topology, Hubbard model, Heisenberg model, and Dzyaloshinskii-Moriya interaction in twisted bilayer WSe_2. *Phys Rev Res*. 2020;2:033 087.
77. Rademaker L. Spin-orbit coupling in transition metal dichalcogenide heterobilayer flat bands. *Phys Rev B*. 2022;105:195 428.
78. Montambaux G, Lim LK, Fuchs JN, Piéchon F. Winding vector: how to annihilate two Dirac points with the same charge. *Phys Rev Lett*. 2018;121:256 402.
79. Yin X, Sarkar S, Shi S, et al. Recent progress in advanced organic electrode materials for sodium-ion batteries: synthesis, mechanisms, challenges and perspectives. *Adv Funct Mater*. 2020;30:1908445.
80. Sajjan M, Sureshbabu SH, Kais S. Quantum machine-learning for eigenstate filtration in two-dimensional materials. *J Am Chem Soc*. 2021;143:18 426-18 445.
81. Sajjan M, Li J, Selvarajan R, et al. Quantum machine learning for chemistry and physics. *Chem Soc Rev*. 2022;51:6475-6573.
82. Sajjan M, Alaeian H, Kais S. Magnetic phases of spatially modulated spin-1 chains in Rydberg excitons: classical and quantum simulations. *J Chem Phys*. 2022;157:224 111.
83. Sajjan M, Singh V, Selvarajan R, Kais S. Imaginary components of out-of-time-order correlator and information scrambling for navigating the learning landscape of a quantum machine learning model. *Phys Rev Res*. 2023;5:013–146.
84. Gupta R, Selvarajan R, Sajjan M, Levine RD, Kais S. Hamiltonian learning from time dynamics using variational algorithms. *arXiv*. Preprint posted online December 28, 2022. doi:arXiv:2212.13702
85. Selvarajan R, Sajjan M, Humble TS, Kais S. Dimensionality reduction with variational encoders based on subsystem purification. *arXiv*. Preprint posted online September 20, 2022. doi:arXiv:2209.09791
86. Li J, Kais S. Entanglement classifier in chemical reactions. *Sci Adv*. 2019;5:eaax5283.
87. Ebadi S, Wang TT, Levine H, et al. Quantum phases of matter on a 256-atom programmable quantum simulator. *Nature*. 2021;595:227-232.
88. Bernien H, Schwartz S, Keesling A, et al. Probing many-body dynamics on a 51-atom quantum simulator. *Nature*. 2017;551:579-584.

SUPPORTING INFORMATION

Additional supporting information can be found online in the Supporting Information section at the end of this article.

How to cite this article: Muruganandam V, Sajjan M, Kais S. Foray into the topology of poly-bi-[8]-annulenylene. *Nat Sci*. 2023;e20230015. https://doi.org/10.1002/ntls.20230015